The Xie Group is grateful to the U.S. Department of Energy's Basic Energy Sciences program (DE-FG02-07ER15875) for supporting high-sensitivity Raman detection. The instrumentation development was supported by NSF (grant DBI-0649892), NIH Director's Pioneer Award (to X.S.X.), the Bill & Melinda Gates Foundation Gates Foundation, and Pfizer Global Medical. Harvard University has filed a patent application based on this work.

Supporting Online Material
www.sciencemag.org/cgi/content/full/322/5909/1857/DC1
Materials and Methods
Figs. S1 to S6
Movies S1 to S3

10 September 2008; accepted 19 November 2008
10.1126/science.1165758

Leukemic Cells Create Bone Marrow Niches That Disrupt the Behavior of Normal Hematopoietic Progenitor Cells

Angela Colmone, Maria Amorim, Andrea L. Pontier, Sheng Wang, Elizabeth Jablonski, Dorothy A. Sipkins*

The host tissue microenvironment influences malignant cell proliferation and metastasis, but little is known about how tumor-induced changes in the microenvironment affect benign cellular ecosystems. Applying dynamic in vivo imaging to a mouse model, we show that leukemic cell growth disrupts normal hematopoietic progenitor cell (HPC) bone marrow niches and creates abnormal microenvironments that sequester transplanted human $CD34^+$ (HPC-enriched) cells. $CD34^+$ cells in leukemic mice declined in number over time and failed to mobilize into the peripheral circulation in response to cytokine stimulation. Neutralization of stem cell factor (SCF) secreted by leukemic cells inhibited $CD34^+$ cell migration into malignant niches, normalized $CD34^+$ cell numbers, and restored $CD34^+$ cell mobilization in leukemic mice. These data suggest that the tumor microenvironment causes HPC dysfunction by usurping normal HPC niches and that therapeutic inhibition of HPC interaction with tumor niches may help maintain normal progenitor cell function in the setting of malignancy.

Hematopoietic progenitor cells (HPCs) home to and engraft in highly specific bone marrow (BM) microenvironments, or niches, that regulate their survival, proliferation, and differentiation (*1*, *2*). These niches have been defined by the association of particular stromal cell types and by their elaboration or secretion of specific signaling molecules, growth factors, and cytokines (*3*). At least two distinct HPC-supportive niches have been identified in the BM: an osteoblastic niche in which molecules including bone morphogenetic protein, osteopontin, angiopoietin-1, and Notch appear to play important regulatory roles; and a vascular niche that remains to be molecularly defined (*4*–*8*).

Although defects in hematopoiesis are frequently observed in patients with malignant involvement of the BM, the molecular bases of these phenomena, and whether they might reflect perturbations in HPC-supportive niches, are unknown. Suppression of normal hematopoiesis can occur in the setting of relatively low tumor burden and thus does not necessarily reflect anatomic "crowding out" of benign cells.

Using a severe combined immunodeficiency (SCID) mouse xenograft model of Nalm-6 pre-B acute lymphoblastic leukemia (ALL), we have shown that malignant cells metastasize to specific stromal cell–derived factor–1 (SDF-1)–positive vascular niches in the BM that overlap with perivascular HPC niches (*9*). To investigate whether benign and malignant cells compete for niche resources, we used real-time, in vivo confocal and multiphoton microscopy imaging approaches that allowed us to colocalize fluorescently labeled BM antigens with fluorescently labeled human $CD34^+$ cells, which are highly enriched in HPCs, and fluorescent tumor cells (*10*). For intravenous transplant into mice, we harvested $CD34^+$ cells from human cord blood and from the peripheral blood of human donors who had been treated

Department of Medicine, Section of Hematology/Oncology, The University of Chicago, 5841 South Maryland Avenue MC 2115, Chicago, IL 60637, USA.

*To whom correspondence should be addressed: E-mail: dsipkins@medicine.bsd.uchicago.edu

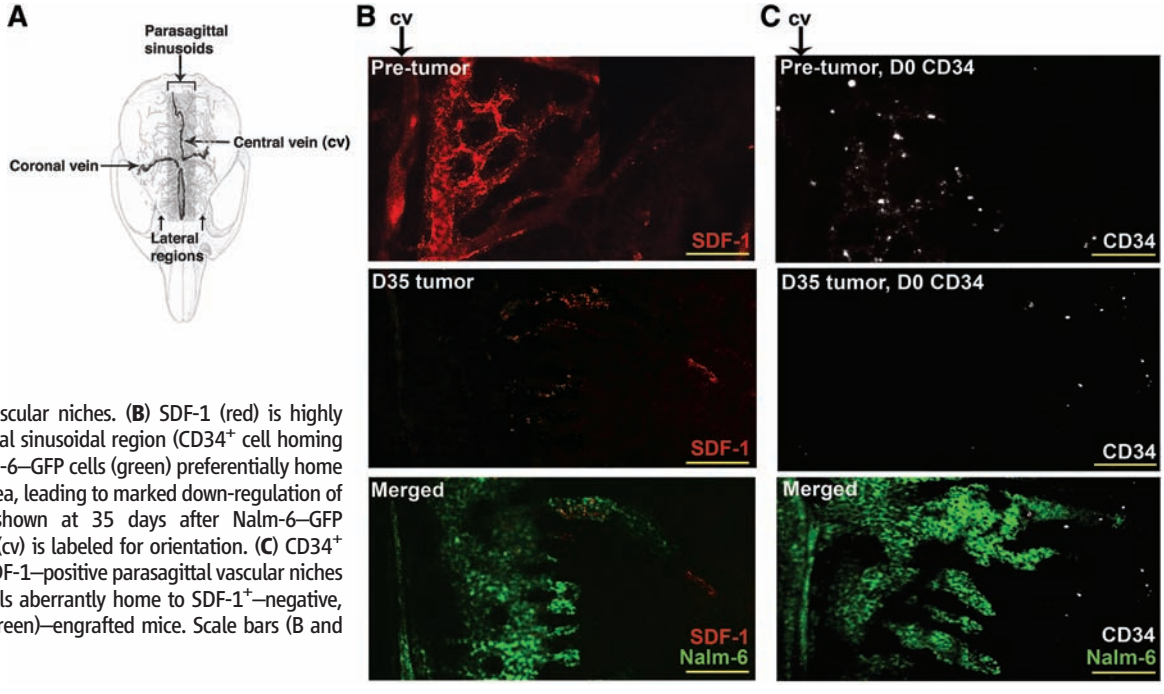

Fig. 1. Leukemia-induced changes in the BM microenvironment disrupt $CD34^+$ cell homing. (**A**) Diagram of mouse calvarial BM vasculature. In control mice, $CD34^+$ cells predominantly home to parasagittal sinusoidal vasculature. A major fraction of $CD34^+$ cells engraft in this parasagittal region after homing, whereas other $CD34^+$ cells migrate to more lateral osteoblastic and vascular niches. (**B**) SDF-1 (red) is highly expressed in the parasagittal sinusoidal region ($CD34^+$ cell homing sites) of control mice. Nalm-6–GFP cells (green) preferentially home to and proliferate in this area, leading to marked down-regulation of SDF-1 expression, here shown at 35 days after Nalm-6–GFP engraftment. Central vein (cv) is labeled for orientation. (**C**) $CD34^+$ cells (white) home to the SDF-1–positive parasagittal vascular niches in control mice. $CD34^+$ cells aberrantly home to SDF-1^+–negative, lateral regions in tumor (green)–engrafted mice. Scale bars (B and C), 250 μm.

Downloaded from http://science.sciencemag.org/ on September 21, 2019

with cytokines to stimulate mobilization of HPCs from the BM. Both of these populations are currently used for therapeutic BM transplantation in humans. Serial imaging of individual mice permitted us to observe cellular migration and proliferation in the calvarial BM over multiple time points from initial BM homing of circulating $CD34^+$ cells through long-term $CD34^+$ cell engraftment (12 weeks or more after transplantation) [Fig. 1A and figs. S1 and S2 (*10*)].

SDF-1 is an important chemoattractant for HPC homing to the BM and plays a key role in maintaining hematopoiesis (*11*–*13*). Because SDF-1 expression is up-regulated in regions of hypoxia or inflammation (*14*, *15*), we hypothesized that SDF-1 protein levels would be increased in the tumor niche. Surprisingly, however, when we assessed the mice for BM SDF-1 expression ~1 month after initial Nalm-6–GFP (green fluorescent protein) engraftment, we found that SDF-1 was markedly down-regulated in regions of heavy tumor growth (Fig. 1B and figs. S3 and S4). These areas of extensive tumor proliferation and SDF-1 down-regulation corresponded to typical $CD34^+$ cell homing niches.

Given that leukemic proliferation occurred preferentially within $CD34^+$ cell homing niches and disrupted chemokine SDF-1 expression at these sites, we next examined whether $CD34^+$ cell BM homing was altered in leukemic mice. Nalm-6–GFP leukemic mice versus control mice were engrafted intravenously with purified, fluorescently labeled human $CD34^+$ cells. Whereas in control mice $CD34^+$ cell homing localized to SDF-1–positive parasagittal vascular niches, in leukemic mice $CD34^+$ cell homing was redirected to atypical lateral microenvironments (Fig. 1C and fig. S5). This finding did not reflect an inability of cells to enter parasagittal regions in leukemic mice, because video-rate imaging confirmed that the cells transited freely through parasagittal tumor-associated vasculature [movies S1 and S2 (*10*)]. Furthermore, when $CD34^+$ cells were pretreated with pertussis toxin (an inhibitor of chemokine receptor $G\alpha_i$-mediated signaling) or with AMD3100 (a small-molecule antagonist of the SDF-1 receptor CXCR4), there was no significant decrease in $CD34^+$ cell homing to the BM in tumor mice (figs. S6 and S7). These data suggest that in leukemic mice, $CD34^+$ cells homed to atypical regions through an SDF-1– and chemokine-independent mechanism.

Although $CD34^+$ cells were able to traffic to BM in leukemic mice, our observation that initial homing occurred in abnormal vascular niches raised the possibility that subsequent engraftment would be altered. We therefore performed serial imaging studies of individual mice to assess the intra-BM movement of $CD34^+$ cells. Surprisingly, most $CD34^+$ cells did not remain at sites of initial homing or migrate to other tumor-free niches. Instead, within days, the vast majority of the transplanted cells aberrantly migrated to SDF-1–negative tumor beds, suggesting that the

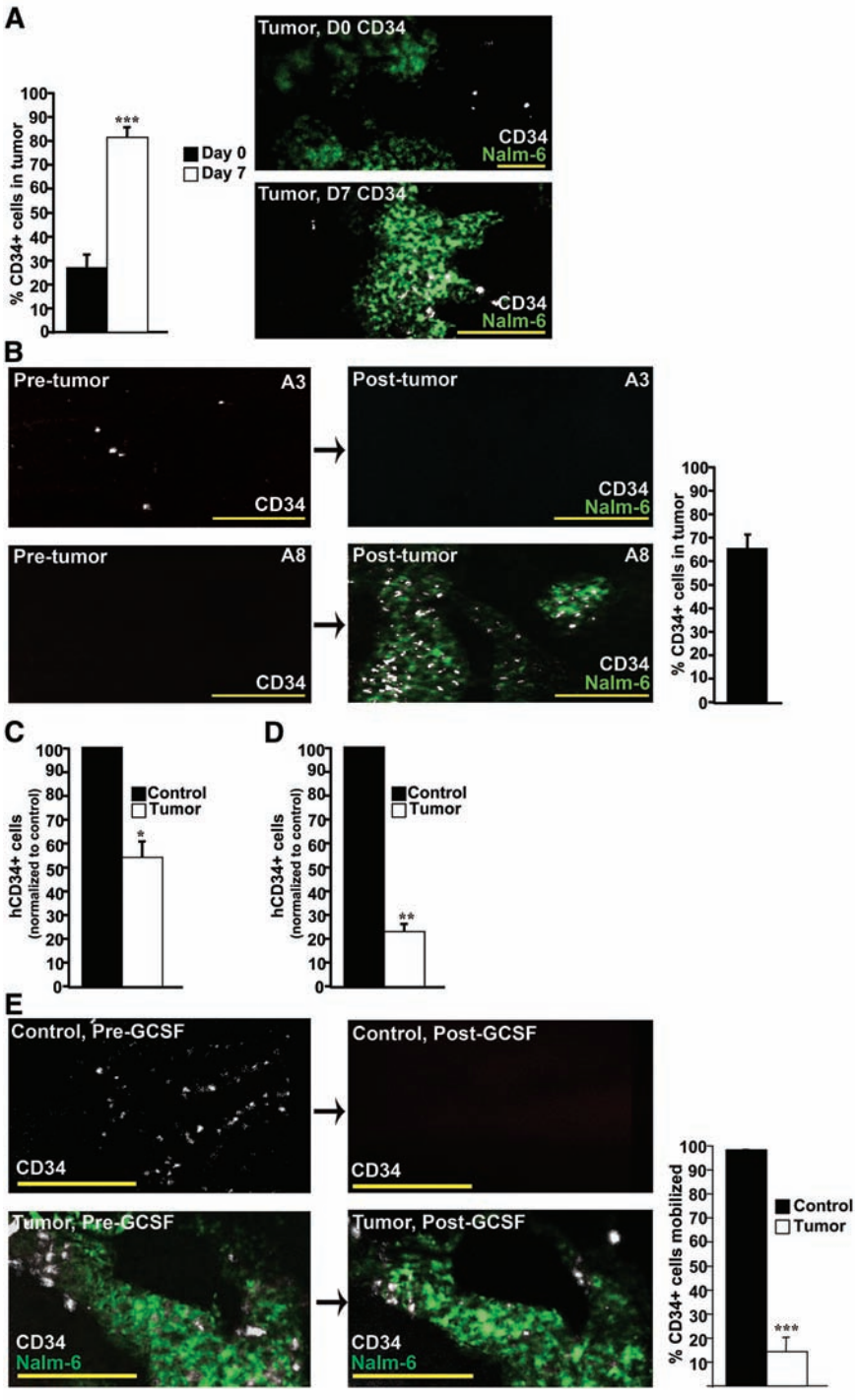

Fig. 2. The malignant microenvironment, or niche, attracts $CD34^+$ cells, but does not maintain $CD34^+$ cell pool size or response to cytokine mobilization. (**A**) Few $CD34^+$ cells colocalize with tumor upon homing to BM (day 0: 25.6 ± 6.7%), yet $CD34^+$ cells migrate into tumor niches over time (day 7: 82.1 ± 4.5%, normalized to total $CD34^+$ cells in BM; $n = 4$ mice, $^{***}P < 0.0001$). (**B**) Serial imaging of mice from 12 to 16 weeks after $CD34^+$ cell (white) transplant reveals that long-term transplanted $CD34^+$ cells abandon normal niches (representative area A3 pretumor) after leukemia (green) engraftment. Conversely, $CD34^+$ cells in leukemic mice migrate to tumor regions (area A8 posttumor) where $CD34^+$ cells do not normally localize. Most of the long-term transplanted $CD34^+$ cells are found within tumor beds (65.9 ± 7%; $n = 6$ mice) in mice imaged ~1 month after tumor engraftment. Tumor involves only 20 to 30% of BM at this time point. (**C** and **D**) Fewer $CD34^+$ cells are harvested from BM of leukemic versus control mice at 7 days (C) [day 7: 55.2 ± 8.5%; $n = 4$ mice (leukemia), $n = 2$ mice (control), $^*P = 0.029$] and 16 weeks (D) (16 weeks: 21.7 ± 3.3%; $n = 4$ (leukemia), $n = 4$ (control), $^{**}P = 0.005$) after $CD34^+$ cell transplant. (**E**) $CD34^+$ cells mobilize from BM upon G-CSF treatment of naïve (98.6 ± 0.2%), but not leukemic (13.8 ± 7%), mice (serial imaging of the same areas; $n = 3$ mice each, leukemia and control, $^{***}P < 0.0005$). Scale bars (A, B, and E), 250 μm.

Downloaded from http://science.sciencemag.org/ on September 21, 2019

tumor had created a new malignant niche capable of recruiting CD34$^+$ cells (Fig. 2A).

To determine if the malignant niche could also compete for CD34$^+$ cells previously established in normal BM niches, we introduced Nalm-6–GFP into mice that had been transplanted with CD34$^+$ cells 12 to 16 weeks earlier. One month after tumor engraftment, most CD34$^+$ cells abandoned tumor-free niches for malignant niches (Fig. 2B). To determine if the malignant niche was able to maintain the new resident CD34$^+$ populations, we harvested human CD34$^+$ cells from leukemic and control mice by magnetic bead selection and quantified the cells by flow cytometry. Significantly fewer CD34$^+$ cells (55.2 ± 8.5%) were recovered from leukemic mice 1 week after CD34$^+$ cell transplantation when compared with control mice (Fig. 2C). In long-term CD34$^+$ cell–transplanted mice subsequently engrafted with leukemia, CD34$^+$ cell counts also declined significantly (21.7 ± 3.3%) over time in leukemic versus control mice (Fig. 2D). These data suggest that the malignant niche, although outcompeting native niches for CD34$^+$ cell localization, fails to preserve the CD34$^+$ cell pool size seen in normal mice.

HPCs are routinely collected for autologous or allogeneic transplant by harvest from the peripheral blood after these cells are mobilized out of the BM by treatment of patients with the cytokine granulocyte colony-stimulating factor (G-CSF). However, the presence of residual BM disease is associated with decreased CD34$^+$ cell mobilization into the peripheral circulation after cytokine treatment (*16*). Addition of the investigational agent AMD3100 to enhance mobilization can also fail to yield adequate stem cell numbers (*17*). Although some of this effect may be related to stromal damage from chemo- and radiotherapy, a clear cause for mobilization failure has not been established (*18*). We therefore examined the effect of malignant niche migration in leukemic mice on CD34$^+$ cell mobilization. CD34$^+$ cells engrafted in leukemic mice minimally mobilized in response to a 5-day course of G-CSF compared with controls (Fig. 2E). Mobilization was not enhanced by the addition of AMD3100 (fig. S8).

We next explored the molecular mechanism responsible for CD34$^+$ cell migration into the malignant niche, with the goal of correcting CD34$^+$ cell dysfunction by inhibiting the transit of these cells from normal microenvironments. To investigate the possibility that the malignant cells might be the source of chemoattractants, we performed transwell migration assays with CD34$^+$ cells and conditioned media (CM) from Nalm-6–GFP, primary human ALL, and primary human acute myeloblastic leukemia (AML) cell cultures. Relative to control media, CD34$^+$ cells migrated in significantly greater numbers (by a factor of 3.5) to leukemia CM (Fig. 3A). Addition of SDF-1 to CM had an additive, but not synergistic, effect on migration (fig. S9). We next screened CM by Western blot for molecules with chemotactic activity for CD34$^+$ cells. Among our initial candidates was stem cell

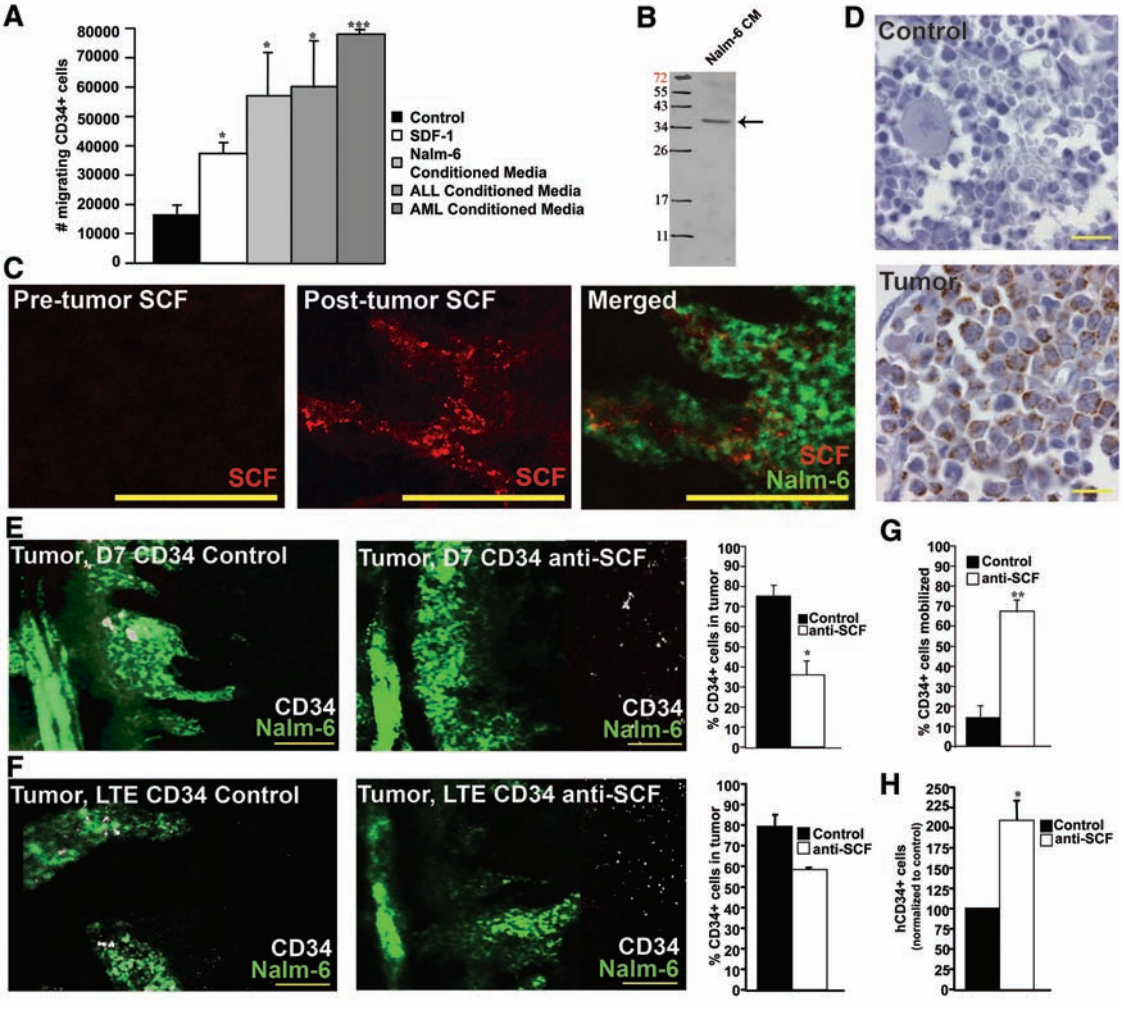

Fig. 3. SCF mediates CD34$^+$ cell migration into the malignant niche, as well as mobilization failure and decrease in CD34$^+$ cell number in leukemic mice. (**A**) CD34$^+$ cells migrate in vitro in response to leukemia-conditioned media (CM). (Control media: 16,137 ± 3799; SDF-1: 37,056 ± 3058; Nalm6-CM: 57,086 ± 14686; ALL-CM: 59,311 ± 17,495; AML-CM: 79,933 ± 933; n = 3 experiments; SDF-1:control, $^*P = 0.0014$; SDF-1:all leukemia-CM, $^*P = 0.009$; SDF-1:Nalm6-CM, $^*P = 0.026$; SDF-1:ALL-CM, $^*P = 0.020$; SDF-1:AML-CM, $^{***}P < 0.0001$). (**B**) SCF protein is secreted by Nalm-6–GFP in vitro. (**C**) In vivo imaging demonstrates increased SCF (red) expression in a tumor (green)–engrafted versus naïve mouse. Scale bars, 250 μm. (**D**) Immunohistochemistry shows hSCF (brown) expression in tumor-engrafted but not control mouse femur. Scale bars, 100 μm. (**E** and **F**) CD34$^+$ cells (white); Nalm-6–GFP (green) (E) Neutralizing treatment with anti-SCF inhibits CD34$^+$ cell migration into tumor 7 days after CD34$^+$ cell transplant into leukemic mice (control: 76.1 ± 5.6%; anti-SCF: 36.7 ± 8.3%; n = 5 mice each, control and anti-SCF, $^*P = 0.008$). Scale bars, 250 μm. (F) Neutralizing anti-SCF inhibits migration of long-term engrafted (LTE) CD34$^+$ cells into the malignant niche. Treatment began 12 weeks after CD34$^+$ cell transplant (at the time of tumor engraftment) and continued for 4 weeks (control: 79.6 ± 6.3%; anti-SCF: 59.3 ± 0.4%; n = 2 mice each, control and anti-SCF). Scale bars, 250 μm. (**G**) Neutralizing anti-SCF restores G-CSF–mediated CD34$^+$ cell mobilization in leukemic mice (control: 13.75 ± 7.0%; anti-SCF: 68.0 ± 6.0%; n = 3 mice each, control and anti-SCF, $^{**}P = 0.004$). (**H**) Seven days after transplant, increased numbers of CD34$^+$ cells were isolated from BM of leukemic mice treated with neutralizing anti-SCF versus control IgG (anti-SCF: 211 ± 23, normalized to control = 100; n = 2 mice each, control and anti-SCF, $^*P = 0.04$).

Downloaded from http://science.sciencemag.org/ on September 21, 2019

factor (SCF), an HPC growth factor and chemoattractant believed to play a role in HSC localization to endosteal niches (*19*–*22*). SCF is produced by a wide variety of solid tumors (*23*–*26*). AML cell lines and primary AML cells have been shown to produce SCF RNA transcripts, but expression of SCF by hematologic malignancies is not well defined (*27*). Figure 3B and fig. S10 show that SCF protein is clearly present in leukemia-CM.

To assess whether SCF expression was up-regulated in the leukemic niche in our mouse model, we performed in vivo immunoimaging of control versus Nalm-6–GFP leukemic mice using fluorescently labeled mouse/human cross-reactive antibodies to SCF (anti-SCF). Whereas only a faint SCF signal was detectable at baseline in control mouse calvarial BM, SCF was highly expressed in mice imaged ~1 month after Nalm-6–GFP engraftment (Fig. 3C). Immunohistochemical staining of mouse femurs confirmed that human SCF (hSCF) was present at high abundance in this marrow compartment (Fig. 3D). In addition, Western blotting of control versus leukemic BM showed expression of human SCF protein product (fig. S11). Quantitative reverse transcription–polymerase chain reaction demonstrated a significant decrease in mouse SCF RNA transcript copy numbers, suggesting that leukemic cells constituted the major source of SCF in the malignant microenvironment (fig. S12).

To determine whether $CD34^+$ cell migration into the malignant niche could be prevented by inhibition of SCF activity, we treated Nalm-6–GFP leukemic mice with SCF-neutralizing antibodies beginning 1 day before $CD34^+$ cell engraftment. We found that at 7 days after $CD34^+$ cell engraftment, significantly fewer $CD34^+$ cells had migrated into tumor niches in treated (37%) versus untreated (76%) mice (Fig. 3E). We also treated long-term $CD34^+$ cell–engrafted mice (12 to 16 weeks) with SCF-neutralizing antibodies beginning 1 day before Nalm-6–GFP engraftment and continuing for 30 days. Again, fewer $CD34^+$ cells exited normal niches for the malignant niche compared with the control (Fig. 3F). To determine if prevention of $CD34^+$ cell egress from benign niches also rescued $CD34^+$ cell function in leukemic mice, we administered a 5-day course of G-CSF (to induce $CD34^+$ cell mobilization) to mice that had been treated with SCF-neutralizing antibody, as well as to control immunoglobulin G (IgG)–treated mice. Sixty-eight percent of $CD34^+$ cells in neutralizing antibody–treated mice mobilized in response to cytokine stimulation versus 14% in untreated mice (Fig. 3G). In another set of experiments, leukemic mice were treated with SCF-neutralizing antibody versus control IgG beginning 1 day before transplant of $CD34^+$ cells. Mice were killed after 7 days for $CD34^+$ cell harvest and quantitation. More than twice as many $CD34^+$ cells were obtained from treated mice (Fig. 3H). These data suggest that $CD34^+$ cell pool size could be maintained in leukemic mice by inhibiting $CD34^+$ cell engagement with the malignant niche.

To extend our observations with the Nalm-6 ALL cell line to primary human disease, we performed similar experiments with cells isolated from BM aspirates of ALL or AML patients. Imaging of mice ~8 weeks after engraftment of primary pre-B ALL or AML in nonobese diabetic–severe combined immunodeficiency (NOD-SCID) mice revealed pronounced up-regulation of SCF signal in the calvarial BM (Fig. 4A and fig. S13). $CD34^+$ cells engrafted in these mice exhibited migration into SCF^+ domains similar to that in Nalm-6–GFP leukemic mice (Fig. 4B). $CD34^+$ cells also failed to respond to G-CSF mobilization (Fig. 4C).

Finally, we determined whether changes in SCF expression could be detected in initial diagnostic BM samples from patients with pre-B ALL. Normal BM biopsies (no evidence of disease) and BM biopsies with known ALL involvement were assayed for SCF by immunohistochemistry of paraffin-embedded sections. As seen in representative micrographs in Fig. 4D, basal expression was low in all three normal controls, whereas SCF staining was markedly elevated (by a factor of 2; Fig. 4E) in all seven patient samples.

We have shown that leukemic proliferation in the BM alters the stromal microenvironment and creates malignant niches that outcompete native HPC niches for $CD34^+$ cell engraftment. Normal $CD34^+$ cells engaged by the malignant niche exhibit abnormal behavior. Our data suggest that therapeutic targeting of SCF may increase the hematopoietic reserve and improve outcomes in BM transplantation and autologous stem cell harvest in the setting of hematologic malignancy. The findings from our xenograft model, however, require confirmation in human studies.

Our results raise many questions about the nature of tumor-host interactions: Do leukemic cells reorganize the molecular microenvironment specifically to entrap HPCs, or is the creation of competitive HPC niches a coincidental side effect of leukemic growth? Conceivably, derangements in hematopoiesis and HPC mobilization could impair anti-tumor immune responses. Of note, SCF neutralization did not significantly inhibit Nalm-6 proliferation in our model, and indeed Nalm-6 cells down-regulate their expression of the SCF receptor, KIT, in vivo (fig. S14). These findings, although not definitive, suggest that Nalm-6 SCF production does not principally serve to fuel autocrine tumor growth. Future studies that elucidate the intricacies of these tumor-host interactions are expected to further our understanding of stem and progenitor cell dysfunction in cancer and expose new therapeutic targets.

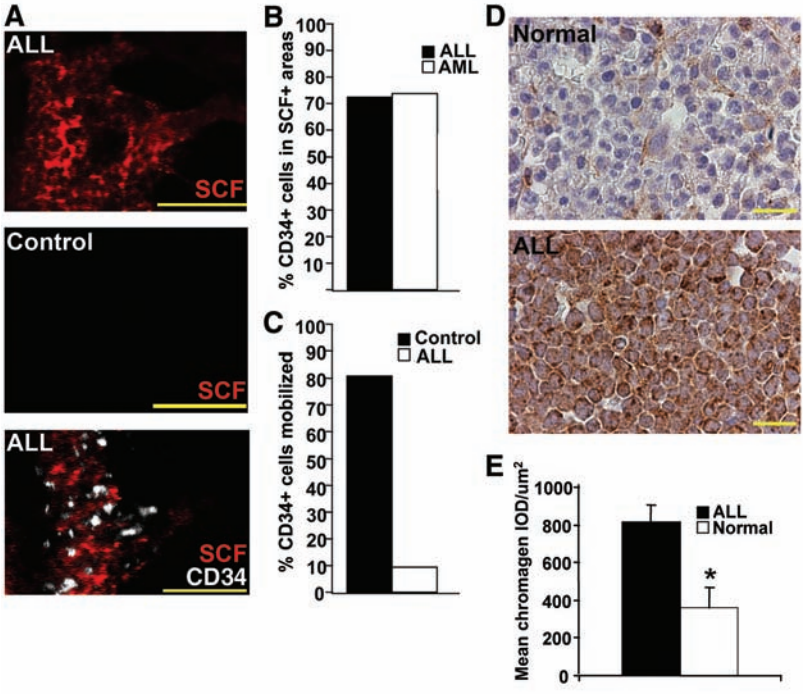

Fig. 4. Primary leukemic cells from patients with ALL and AML create abnormal $CD34^+$ cell niches; human ALL BM biopsies demonstrate marked up-regulation of SCF. (**A**) SCF (red) expression is markedly up-regulated in ALL-engrafted versus control mice. $CD34^+$ cells (white) localize to regions of high SCF expression. Scale bars, 250 μm. (**B**) $CD34^+$ cells migrate into the malignant niche in ALL and AML-engrafted mice (ALL: 72.7%; AML: 73.6%). (**C**) $CD34^+$ cells do not respond to G-CSF mobilization in ALL-engrafted mice (control: 80.4%, ALL: 7.8%). (**D**) Representative micrographs of SCF (brown) immunohistochemical staining in a diagnostic BM biopsy from a patient with pre-B ALL versus a normal BM biopsy. Scale bars, 100 μm. (**E**) Quantitative analysis of SCF immunostaining intensity in ALL versus normal BM biopsies (ALL: 814 ± 88, n = 7 patients; normal: 364 ± 107, n = 3 patients; *P = 0.004).

References and Notes

1. O. Naveiras, G. Q. Daley, *Cell. Mol. Life Sci.* **63**, 760 (2006).
2. H. G. Kopp, S. T. Avecilla, A. T. Hooper, S. Rafii, *Physiology (Bethesda)* **20**, 349 (2005).
3. T. Yin, L. Li, *J. Clin. Invest.* **116**, 1195 (2006).
4. J. Zhang *et al.*, *Nature* **425**, 836 (2003).
5. S. K. Nilsson *et al.*, *Blood* **106**, 1232 (2005).
6. F. Arai *et al.*, *Cell* **118**, 149 (2004).
7. L. M. Calvi *et al.*, *Nature* **425**, 841 (2003).

Downloaded from http://science.sciencemag.org/ on September 21, 2019

8. M. J. Kiel, O. H. Yilmaz, T. Iwashita, C. Terhorst, S. J. Morrison, *Cell* **121**, 1109 (2005).
9. D. A. Sipkins *et al.*, *Nature* **435**, 969 (2005).
10. Materials and methods are available as supporting material on *Science* Online.
11. A. Peled *et al.*, *Science* **283**, 845 (1999).
12. T. Lapidot, O. Kollet, *Leukemia* **16**, 1992 (2002).
13. H. E. Broxmeyer, *Curr. Opin. Hematol.* **15**, 49 (2008).
14. D. J. Ceradini *et al.*, *Nat. Med.* **10**, 858 (2004).
15. C. Hitchon *et al.*, *Arthritis Rheum.* **46**, 2587 (2002).
16. B. Nervi, D. C. Link, J. F. DiPersio, *J. Cell. Biochem.* **99**, 690 (2006).
17. G. Calandra *et al.*, *Bone Marrow Transplant.* **41**, 331 (2008).
18. W. Bensinger *et al.*, *J. Clin. Oncol.* **13**, 2547 (1995).
19. N. Okumura *et al.*, *Blood* **87**, 4100 (1996).
20. R. L. Driessen, H. M. Johnston, S. K. Nilsson, *Exp. Hematol.* **31**, 1284 (2003).
21. L. K. Ashman, *Int. J. Biochem. Cell Biol.* **31**, 1037 (1999).
22. S. Sharma *et al.*, *Stem Cells Dev.* **15**, 755 (2006).
23. N. Théou-Anton *et al.*, *Br. J. Cancer* **94**, 1180 (2006).
24. K. A. Giehl, U. Nagele, M. Vokenandt, C. Berking, *J. Cutan. Pathol.* **34**, 7 (2007).
25. G. Bellone *et al.*, *Int. J. Oncol.* **29**, 851 (2006).
26. M. Tao *et al.*, *Cytokine* **12**, 699 (2000).
27. R. Zheng, K. Klang, N. C. Gorin, D. Small, *Leuk. Res.* **28**, 121 (2004).

28. We thank A. Chenn, K. Cohen, L. Godley, and R. Salgia for critical discussions and reading of the manuscript; A. Chenn for assistance with retroviral cell transduction; A. Wickrema for help with CD34$^+$ purification; V. Bindokas for imaging expertise; and S. Gurbuxani for assistance with histopathology interpretation. Supported by a grant from the Illinois Regenerative Medicine Institute (IRMI), an NIH (National Cancer Institute) K08 award (5K08CA112126-02), and an NIH Director's DP2 award (1DP2OD002160-01). A patent application related to this work has been filed by the University of Chicago.

Supporting Online Material

www.sciencemag.org/cgi/content/full/322/5909/1861/DC1
Materials and Methods
Figs. S1 to S13
Movies S1 and S2

7 August 2008; accepted 19 November 2008
10.1126/science.1164390

Representation of Geometric Borders in the Entorhinal Cortex

Trygve Solstad, Charlotte N. Boccara,* Emilio Kropff,* May-Britt Moser, Edvard I. Moser†

We report the existence of an entorhinal cell type that fires when an animal is close to the borders of the proximal environment. The orientation-specific edge-apposing activity of these "border cells" is maintained when the environment is stretched and during testing in enclosures of different size and shape in different rooms. Border cells are relatively sparse, making up less than 10% of the local cell population, but can be found in all layers of the medial entorhinal cortex as well as the adjacent parasubiculum, often intermingled with head-direction cells and grid cells. Border cells may be instrumental in planning trajectories and anchoring grid fields and place fields to a geometric reference frame.

An animal's current position in the environment is encoded by a network of hippocampal and parahippocampal neurons with diverse spatial firing properties. Within this network, at least three cell types contribute to the computation of self-location: place cells, which fire when the animal moves through a particular location in space (*1*–*3*); head-direction cells, which fire when the animal is facing in a certain direction (*4*–*7*); and grid cells, whose multiple sharply localized firing fields form a remarkably regular triangular pattern across the environment (*3*, *7*–*9*). In addition to these cell types, computational models posit the existence of cortical "boundary vector cells," whose activity patterns encode the animal's distance from salient geometric borders (*10*, *11*). Based on predictions from these models, we investigated whether proximity to borders is represented by specific cell types in the entorhinal spatial representation circuit (*12*).

A total of 624 principal cells were recorded from the dorsocaudal quarter of the medial entorhinal cortex (MEC) and adjacent parasubiculum in 13 rats (fig. S1). Neural activity was sampled while these animals foraged in enclosures with moveable walls and barriers. The animals were first tested in a square enclosure (1 m by 1 m or 1.5 m by 1.5 m) with 50-cm-high walls. Many recorded cells were grid cells and head-direction cells (*7*–*9*), but in addition the data included a previously unknown class of entorhinal cells that fired exclusively along one or several walls of the enclosure (Fig. 1 and fig. S2). These cells were identified by computing, for each cell, the difference between the maximal length of a wall touching upon a single firing field and the average distance of the fields from the nearest wall, divided by the sum of those values (*12*). Border scores ranged from –1 for cells with central firing fields to +1 for cells with fields that perfectly lined up along at least one entire wall. "Border cells" were defined as spatially stable cells with border scores above 0.5. A total of 69 cells from 12 animals passed this criterion (Fig. 1 and fig. S2) (*13*). In these cells, 86.0 ± 0.6% of the spikes occurred closer to the walls than to the center of the box per unit of time [mean ± SEM; $t(68) = 17.4$, one-sample t test, $P < 0.001$; expected value 75%]. Only 3.6 ± 1.0% of the

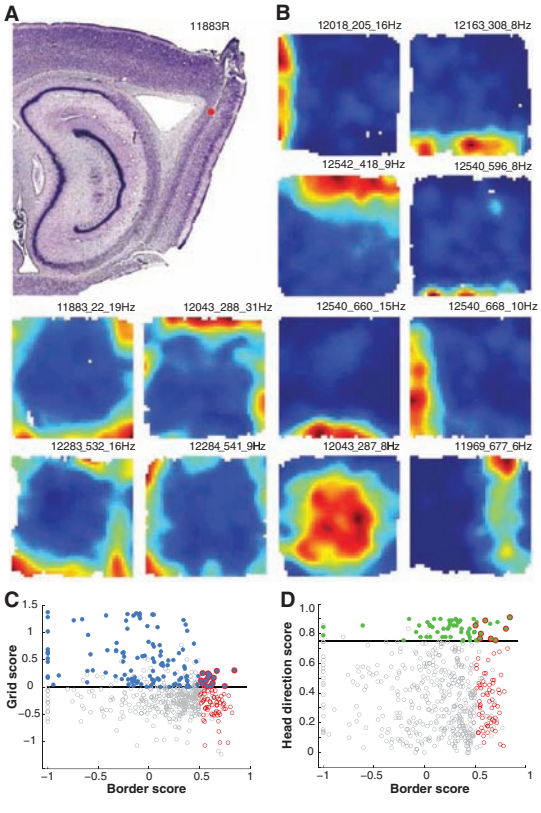

Fig. 1. Examples of border cells in the MEC and adjacent parasubiculum. (**A**) Sagittal Nissl-stained section showing a representative recording location in the MEC (red dot, recording location; rat number and hemisphere (R, right) are indicated; see fig. S1 for all other recording positions). (**B**) Color-coded rate maps for 12 border cells. Red is maximum, dark blue is zero. Pixels not covered are white. Animal numbers (five digits), cell numbers (two or three digits), and peak firing rates are indicated above each panel. Cells 287 and 677 did not pass the criterion for border cells because the fields were located at some distance from the wall; the number of such cells was fewer than 10. See fig. S2 for the complete set of rate maps, trajectories, and directional tuning curves, and representative waveforms and tetrode clusters. (**C** and **D**) Scatter plots showing correlation between border scores and grid scores (C) or head-direction scores (D) (*12*). Each dot in the scatter plot corresponds to one cell (red, border cells; blue, grid cells; green, head-direction cells; gray, cells not passing any criterion, including cells with high spatial or directional scores but low stability; double-colored dots, cells that satisfy criteria for two cell classes). Horizontal lines indicate thresholds for grid and head-direction cells.

Kavli Institute for Systems Neuroscience and Centre for the Biology of Memory, Norwegian University of Science and Technology, 7489 Trondheim, Norway.

*These authors contributed equally to this work.
†To whom correspondence should be addressed. E-mail: edvard.moser@ntnu.no

Downloaded from http://science.sciencemag.org/ on September 21, 2019

Science

Leukemic Cells Create Bone Marrow Niches That Disrupt the Behavior of Normal Hematopoietic Progenitor Cells

Angela Colmone, Maria Amorim, Andrea L. Pontier, Sheng Wang, Elizabeth Jablonski and Dorothy A. Sipkins

Science **322** (5909), 1861-1865.
DOI: 10.1126/science.1164390

ARTICLE TOOLS http://science.sciencemag.org/content/322/5909/1861

SUPPLEMENTARY MATERIALS http://science.sciencemag.org/content/suppl/2008/12/18/322.5909.1861.DC1

RELATED CONTENT http://stke.sciencemag.org/content/sigtrans/1/51/ec443.abstract

REFERENCES This article cites 26 articles, 4 of which you can access for free
http://science.sciencemag.org/content/322/5909/1861#BIBL

PERMISSIONS http://www.sciencemag.org/help/reprints-and-permissions

Use of this article is subject to the Terms of Service

Science (print ISSN 0036-8075; online ISSN 1095-9203) is published by the American Association for the Advancement of Science, 1200 New York Avenue NW, Washington, DC 20005. The title *Science* is a registered trademark of AAAS.

American Association for the Advancement of Science

Downloaded from http://science.sciencemag.org/ on September 21, 2019